

# Effects of simulated Secondary Organic Aerosol Water on PM<sub>1</sub> levels and composition over US

Stylianos Kakavas<sup>1,2</sup>, Spyros N. Pandis<sup>1,2</sup> and Athanasios Nenes<sup>1,3</sup>

<sup>1</sup>Institute of Chemical Engineering Sciences, Foundation for Research and Technology Hellas, Patras, Greece

<sup>2</sup>Department of Chemical Engineering, University of Patras, Patras, Greece

<sup>3</sup>School of Architecture, Civil and Environmental Engineering, École Polytechnique Fédérale de Lausanne (EPFL), Switzerland

*Correspondence to:* Athanasios Nenes ([athanasios.nenes@epfl.ch](mailto:athanasios.nenes@epfl.ch)) and Spyros N. Pandis ([spyros@chemeng.upatras.gr](mailto:spyros@chemeng.upatras.gr)).

**Abstract.** Water is a key component of atmospheric aerosol, affecting many aerosol processes including gas/particle partitioning of semi-volatile compounds. Water related to secondary organic aerosol (SOAW) is often neglected in atmospheric chemical transport models and is not considered in gas-to-particle partitioning calculations for inorganic species. We use a new inorganic aerosol thermodynamics model, ISORROPIA-lite, which considers the effects of SOAW, to perform chemical transport model simulations for a year over the continental United States to quantify its effects on aerosol mass concentration and composition. SOAW can increase average fine aerosol water levels up to a factor of two when secondary organic aerosol (SOA) is a major PM<sub>1</sub> component. This is often the case in the south-eastern U.S where SOA concentrations are higher. Although the annual average impact of this added water on total dry PM<sub>1</sub> concentrations due to increased partitioning of nitrate and ammonium is small (up to 0.1  $\mu\text{g m}^{-3}$ ), total dry PM<sub>1</sub> increases of up to 2  $\mu\text{g m}^{-3}$  (with nitrate levels increases up to 200%) can occur when RH levels and PM<sub>1</sub> concentrations are high.

## 1. Introduction

Atmospheric particulate matter with aerodynamic diameter smaller than 1  $\mu\text{m}$  (PM<sub>1</sub>) has adverse effects on public health, climate and ecosystem productivity (Pye et al., 2020; Baker et al., 2021; Guo et al., 2021). PM<sub>1</sub> is composed of thousands of organic compounds, black carbon (BC), and inorganic components such as sulfate (SO<sub>4</sub><sup>2-</sup>),

35 nitrate ( $\text{NO}_3^-$ ), ammonium ( $\text{NH}_4^+$ ) and chloride ( $\text{Cl}^-$ ) (Seinfeld and Pandis, 2006).  
36 Ambient aerosol is mostly composed of water which is determined by the chemical  
37 equilibrium of water vapor with the aerosol constituents (Liao and Seinfeld, 2005;  
38 Carlton and Turpin, 2013; Bian et al., 2014; Guo et al., 2015; Bougiatioti et al., 2016;  
39 Nguyen et al., 2016; Guo et al., 2017; Deetz et al., 2018; Kuang et al., 2018; Song et  
40 al., 2018; Wu et al., 2018; Pye et al., 2020; Gopinath et al., 2022). Aerosol liquid water  
41 directly affects the PM sensitivity and dry deposition rates, with direct implications for  
42 emissions control policy (Nenes et al., 2020; Nenes et al., 2021; Sun et al., 2021).

43 The hygroscopicity parameter ( $\kappa$ ), which expresses the ability of a PM  
44 component to absorb water, is an effective approach for the parameterization of the  
45 water uptake of atmospheric PM that is a mixture of organic and inorganic species  
46 (Petters and Kreidenweis, 2007). Although organic aerosol (OA) is less hygroscopic  
47 than inorganic salts, it can still contribute significantly to the total aerosol water (Guo  
48 et al., 2015; Bougiatioti et al., 2016; Jathar et al., 2016; Li et al., 2019) or can even  
49 become the dominant contributor at lower ambient relative humidity (Jin et al., 2020).  
50 Previous studies have demonstrated that secondary organic aerosol (SOA) is a lot more  
51 hygroscopic ( $0.1 \leq \kappa \leq 0.3$ ) than primary organic aerosol (POA) ( $\kappa \leq 0.01$ ) and is mainly  
52 responsible for the corresponding OA water (Petters et al., 2006; Koehler et al., 2009;  
53 Chang et al., 2010; Jathar et al., 2016; Kuang et al., 2020; Li et al., 2020).

54 SOAW can enhance secondary inorganic aerosol concentrations assisting in  
55 their partitioning in the particulate phase to satisfy equilibrium. However, such effects  
56 are not considered in thermodynamic modules used for the simulation of gas-to-particle  
57 partitioning of inorganic species in chemical transport models. Evidence exists however  
58 that fine aerosol nitrate and ammonium concentrations can increase in areas with high  
59 organic aerosol and RH levels (Kakavas et al., 2022). The importance of these SOAW  
60 impacts on secondary aerosol formations has not been systematically studied and is the  
61 focus of this work.

62 We use a new aerosol thermodynamics model, ISORROPIA-lite (Kakavas et  
63 al., 2022), to simulate SOAW effects on the partitioning of the inorganic components,  
64 for a year over the continental United States. The model performance has been  
65 evaluated for fine PM and its components for the examined period by Skyllakou et al.  
66 (2021). It is considered good for the total  $\text{PM}_{2.5}$  concentration and average for most of  
67 the components. The aim of our work is to quantify the SOAW contribution to the total

68 fine PM water and to study its effects on inorganic aerosol thermodynamics and total  
69 dry fine PM levels and composition.

70

## 71 **2. Methods**

### 72 **2.1 ISORROPIA-lite**

73 ISORROPIA-lite is a lean and accelerated version of the widely used ISORROPIA-II  
74 (Fountoukis and Nenes, 2007) aerosol thermodynamics model and it focuses on the  
75 simulation of the composition of the inorganic fraction of the atmospheric aerosol that  
76 is in equilibrium with the gas phase. It assumes that the aerosol exists only in the  
77 metastable state at low RH and the activity coefficients of ionic pairs are always  
78 obtained from precalculated look-up tables. It estimates aerosol water associated with  
79 each one of the aerosol components. Furthermore, ISORROPIA-lite has an important  
80 additional feature compared to ISORROPIA-II, as it considers the effects of SOAW on  
81 inorganic aerosol thermodynamics. The resulting increase of the total water mass drives  
82 more of the water-soluble gaseous species to the particle phase to satisfy equilibrium.  
83 SOAW,  $W_{SOA}$ , in ISORROPIA-lite is calculated using the well-established  $\kappa$ -Kohler  
84 theory of Petters and Kreidenweis (2007):

$$85 \quad W_{SOA} = \frac{\rho_w}{\rho_{SOA}} \frac{C_{SOA} \kappa}{\left(\frac{1}{RH} - 1\right)} \quad (1)$$

86 where  $\rho_w$  is the density of water,  $\rho_{SOA}$  the SOA density,  $C_{SOA}$  the SOA concentration,  $\kappa$   
87 the SOA hygroscopicity parameter and RH the relative humidity in the 0–1 scale. More  
88 details about the ISORROPIA-lite can be found in Kakavas et al. (2022).

89

### 90 **2.2 PMCAMx description and application**

91 PMCAMx (Karydis et al., 2010; Tsimpidi et al., 2010) is a three dimensional chemical  
92 transport model based on CAMx (Environ, 2006), which simulates horizontal and  
93 vertical advection and dispersion, dry and wet deposition, as well as aqueous, gas, and  
94 aerosol chemistry. The mechanism used in this work for gas-phase chemistry  
95 simulations is the Carbon Bond 05 (CB5) (Yarwood et al., 2005) and includes 190  
96 reactions of 79 gas species. To describe the aerosol size and composition distribution  
97 10-size sections (from 40 nm to 40  $\mu$ m) are used assuming that all particles in each size  
98 bin have the same composition. Therefore, PMCAMx predicts  $PM_x$  concentrations  
99 where  $x$  can be among other choices 1, 2.5 and 10  $\mu$ m. Equilibrium is always assumed

100 between the bulk aerosol and gas phases. The partitioning of semi-volatile inorganic  
101 species between the gas and particulate phases is simulated by ISORROPIA-lite.  
102 Weighting factors based on the effective surface area of each size bin are used to  
103 distribute to the various size bins the mass transferred between the two phases in each  
104 time step (Pandis et al., 1993). For the simulation of organic aerosols, the volatility  
105 basis set (VBS) approach (Donahue et al., 2006) is used. POA is simulated using eight  
106 volatility bins (from  $10^{-1}$  to  $10^6 \mu\text{g m}^{-3}$ ) at 298 K, while for SOA four volatility bins (1,  
107  $10, 10^2, 10^3 \mu\text{g m}^{-3}$ ) at 298 K are used (Murphy and Pandis, 2009). An organic aerosol  
108 phase is assumed with its components forming a pseudo-ideal solution and being in  
109 equilibrium with the gas phase (Strader et al., 1998). The influence of water on the  
110 partitioning of the organic components of the particulate matter between the gas and  
111 aerosol phases is assumed to be negligible in this version of PMCAMx (Koo et al.,  
112 2003). The low volatility organic compounds (LVOCs) and the extremely LVOCs are  
113 implicitly included in the lowest volatility bin of this version of the VBS used in  
114 PMCAMx. These compounds are always in the particulate phase in these simulations  
115 and therefore the addition of lower bins increases the computational cost without  
116 changing the predicted organic aerosol concentration. For the major point sources, the  
117  $\text{NO}_x$  plumes are simulated using the Plume-in-Grid (PiG) approach (Karamchandani et  
118 al., 2011; Zakoura and Pandis, 2019). The variable size resolution model (VSRM) of  
119 Fahey and Pandis (2001) is used for the simulation of aqueous-phase. The model is  
120 based on the chemical mechanism of Pandis and Seinfeld (1989) with the addition of  
121  $\text{Ca}^{2+}$  to the list of particle components as well as  $\text{H}_2\text{SO}_4$  in the gas phase (Fahey and  
122 Pandis, 2001).

123 We applied PMCAMx over the continental United States during 2010. The  
124 modeling domain includes northern Mexico and southern Canada and covers a  $4752 \times$   
125  $2952 \text{ km}^2$  region (Figure S1). The model grid consists of 10,824 cells with horizontal  
126 dimensions of  $36 \times 36 \text{ km}$ . The meteorological inputs were provided by the Weather  
127 Research Forecasting model (WRF v3.6.1) using a horizontal resolution of  $12 \times 12 \text{ km}$ .  
128 RH levels above 95% were rare therefore there was no need for screening of the few  
129 high RH values outside clouds. The gaseous and primary particle emissions were  
130 developed by Xing et al. (2013). More details about the meteorological inputs and the  
131 emissions can be found in Skyllakou et al. (2021).

132 To quantify the SOAW effects on inorganic aerosol thermodynamics three  
133 simulations were performed. The first was a simulation neglecting SOAW and

134 including only inorganic aerosol water. Two additional simulations were performed:  
135 one where  $\kappa$  of SOA was assumed to be equal to 0.1 and one with  $\kappa=0.2$  (Kuang et al.,  
136 2020) to examine how SOA hygroscopicity affects total fine aerosol water content and  
137 PM levels and composition. Even if higher values of the hygroscopicity parameter (e.g.,  
138  $\kappa=0.3$ ) are possible (Kuang et al., 2020) these represent rather extreme cases for the  
139 simulation of the average effects over the US. Therefore, the two simulations used in  
140 this study provide a good estimate of the corresponding uncertainty. Previous studies  
141 have estimated secondary organic aerosol density values of 1–1.4 g cm<sup>-3</sup> (Turpin and  
142 Lim, 2001; Kostenidou et al., 2007). A SOA density of 1 g cm<sup>-3</sup> was assumed in the  
143 simulations. The SOA exists mostly in submicrometer particles so our subsequent study  
144 focuses on PM<sub>1</sub>.

145

### 146 **3. Results**

#### 147 **3.1 Effects of SOAW on PM<sub>1</sub> water levels**

148 The annual average PM<sub>1</sub> water ground-level concentrations neglecting SOAW are  
149 shown in Figure 1. Higher PM<sub>1</sub> water concentrations from 8 to 18 μg m<sup>-3</sup> are predicted  
150 in the north-eastern part of the US due to the higher inorganic PM<sub>1</sub> concentrations  
151 (Figure 2) and RH levels in that area. When SOAW is present in the simulations, total  
152 PM<sub>1</sub> water levels increase everywhere with higher fractional increases in the south-  
153 eastern US (up to 50% when  $\kappa=0.1$  and up to 100% when  $\kappa=0.2$  in Alabama and north-  
154 western Mexico) due to higher SOA levels (Figure S2). In the north-eastern US, lower  
155 fractional increases are predicted (10–15% when  $\kappa=0.1$  and 20–30% when  $\kappa=0.2$ ). In  
156 general, assuming a  $\kappa$  of SOA equal to 0.2 instead of 0.1 increases the corresponding  
157 amount of SOAW by about a factor of two. Figure 1 shows the distributions of  
158 fractional increase change in the annual PM<sub>1</sub> water levels at ground level from SOAW.  
159 Total PM<sub>1</sub> water average concentrations increase from 20 to 30% in about 60% of the  
160 modeling domain when  $\kappa=0.1$ . For  $\kappa=0.2$ , the corresponding increase is from 40 to 60%.

161 Predicted SOA levels are higher during summertime (Figure S2) since the  
162 emissions and oxidation rates of volatile organic compounds (VOCs) are higher (Zhang  
163 et al., 2013; Freney et al., 2014; Skyllakou et al., 2014; Fountoukis et al., 2016).  
164 However, even during wintertime fresh biomass burning emissions exposed to NO<sub>2</sub> and  
165 O<sub>3</sub> can form significant amounts of SOA in periods with low OH levels (Kodros et al.,  
166 2020). Higher total PM<sub>1</sub> water concentrations are predicted during winter (Figure 3)  
167 since the RH levels and inorganic fine aerosol concentrations are higher; especially

168 nitrate and chloride which increasingly partition to the aerosol phase as temperature  
169 decreases (Guo et al., 2017). However, PM<sub>1</sub> chloride concentrations are low (less than  
170 0.1 μg m<sup>-3</sup>) with higher concentrations in Kansas because of biomass burning episodes.  
171 Higher fractional increases in fine aerosol water levels (up to 5 times) due to SOAW  
172 are predicted during summer in the south-eastern part of US where SOA concentrations  
173 are higher. This corresponds to increases to average fine aerosol water concentrations  
174 up to 8 μg m<sup>-3</sup>.

175 Ammonium nitrate and ammonium sulfate are the inorganic salts that contribute  
176 the most to the total PM<sub>1</sub> water levels (Figure S3). SOAW also contributes significantly  
177 to the total PM<sub>1</sub> water levels especially in the south-eastern US (about 30 and 50% of  
178 total PM<sub>1</sub> water when κ=0.1 and κ=0.2 respectively), when the mass fraction of SOA  
179 in dry PM<sub>1</sub> exceeds 30%.

180

### 181 **3.2 Effects of SOAW on total dry PM<sub>1</sub> levels**

182 Higher dry PM<sub>1</sub> concentrations are predicted for the eastern part of the US (up to 15 μg  
183 m<sup>-3</sup>) in the base case (Figure 4). These dry PM<sub>1</sub> levels increase slightly up to 0.6% and  
184 1.2% due to SOAW when κ=0.1 and κ=0.2 for SOA is assumed. The highest annual  
185 average fractional increase in total dry PM<sub>1</sub> levels is predicted in California (1% when  
186 κ=0.1 and 2% when κ=0.2). The probability density (Figure 4) indicates that in about  
187 60% of the modeling domain total dry fine aerosol concentrations increase up to 0.3%  
188 when κ=0.1. For κ=0.2, the corresponding increase is from 0.4 to 2%. The areas of the  
189 highest PM<sub>1</sub> increase correspond to regions where aerosol pH tends to be relatively high  
190 (Pye et al., 2020). In these areas, nitric acid and ammonia can condense and increase  
191 aerosol mass because of the increase in water from the SOA. Because of this  
192 partitioning change, the predicted gas-phase concentrations of semi-volatile inorganic  
193 components decreased on average when SOAW was considered (Figure S4). SOAW  
194 had a negligible absolute impact on the small fine chloride concentrations in this period  
195 (Figure 2). However, in periods during which chloride salts and SOA contribute  
196 significantly to the total dry (e.g. during intense biomass burning periods), fine chloride  
197 concentrations could also change (Metzger et al., 2006; Fountoukis et al., 2009; Gunthe  
198 et al., 2021).

199 Skyllakou et al. (2021) found that PMCAMx had a small fractional bias (5%)  
200 and a fractional error (25%) for the annual average PM<sub>2.5</sub> concentrations of 1067  
201 measurements stations in the U.S. The performance of PMCAMx regarding annual

202 average OA is considered good in these simulations with a fractional bias of 5% and a  
203 fractional error of 26% in the 306 stations in the US. For daily average concentrations  
204 the performance is also quite encouraging with a fractional bias of 15% and a fractional  
205 error of 56%. Given that the effect of the extension of the model on the total fine PM  
206 mass is small (of the order of 1%), this does not result in any noticeable change in its  
207 already very good performance for dry fine PM. Therefore, the major change in the  
208 model predictions is on the aerosol water concentrations.

209

### 210 **3.3 Effects of SOAW on PM<sub>1</sub> components**

211 The annual average results indicate that SOAW mainly affects fine aerosol water levels.  
212 To better analyze the effects of SOAW we focus on the temporal evolution of the  
213 predicted levels of PM<sub>1</sub> components in four sites (Figure S1) with different  
214 characteristics (Table S1). We have chosen one city from the West, one from the South,  
215 one from Southeast and one from the Northeast. They are all in different environments  
216 with different major sources and climatological conditions. The presence of SOAW  
217 increased PM<sub>1</sub> water concentrations in all sites from 1% to almost an order of  
218 magnitude (Figure 5). However, these fractional increases most of the time correspond  
219 to PM<sub>1</sub> water concentration increases of a few  $\mu\text{g m}^{-3}$  (Figure S5) because they occur  
220 under low RH levels. During higher RH periods (80 to 100%), the PM<sub>1</sub> water levels are  
221 predicted to increase up to  $100 \mu\text{g m}^{-3}$  (e.g. in Toronto).

222 Total dry PM<sub>1</sub> concentrations during most of the simulated period increase on  
223 average less than 1% in all sites (Figure 5) due to SOAW. There are periods, however,  
224 with higher fractional increases (up to 10%) and even small decreases (up to 5%) in  
225 total dry fine aerosol levels in the examined sites. The decreases can be explained  
226 because SOAW increases the size of particles and therefore their dry deposition rate  
227 (Nenes et al., 2020). Depending on SOA hygroscopicity, increases up to  $1.5 \mu\text{g m}^{-3}$  for  
228 nitrate and  $0.5 \mu\text{g m}^{-3}$  for ammonium are predicted (Figure S5). Fine nitrate increases  
229 of 10% were more frequent in the examined sites; however higher increases up to 200%  
230 are predicted during the simulated period (Figure 6). As expected, higher increases can  
231 occur more often with higher assumed SOA hygroscopicity.

232

## 233 **4. Discussion**

234 Aerosol liquid water has a profound impact on aerosol processes, chemical composition  
235 and their impacts. By including the effects of organic water on inorganics

236 thermodynamic equilibrium we show that SOAW can substantially increase aerosol  
237 water levels, on an average up to 60% over the majority of the domain. As a  
238 consequence, total dry PM<sub>1</sub> levels can also increase but the changes are small (up to 2%  
239 on an annual average basis). Locally these effects can be much more significant during  
240 periods of high RH and SOA levels (fine nitrate fractional increases can be as high as  
241 200%).

242 The effects vary with season. During summer, the RH is lower and SOA levels  
243 are higher leading to higher fractional increases in aerosol water (Figure 3) but lower  
244 absolute mass changes. During summer the fractional increases in total dry fine aerosol  
245 concentrations are lower than in wintertime (Figure S6). Responsible for the total dry  
246 fine aerosol concentration increases are nitrate and ammonium (Figure 2). These  
247 compounds partition together (as deliquesced ammonium nitrate) to the particulate  
248 phase to satisfy equilibrium due to the additional water mass of SOA.

249 The increases in total dry PM<sub>1</sub> and fine aerosol water levels depend on SOA  
250 concentrations, hygroscopicity value, RH levels and the particle phase fractions of  
251 inorganic species. The SOAW effect on aerosol water is approximately proportional to  
252 the assumed hygroscopicity parameter  $\kappa$ . Given that our work investigates the potential  
253 significance of this effect we have chosen to provide the results of two simulations one  
254 with relatively low and relatively high hygroscopicity of SOA. A more detailed  
255 treatment of the hygroscopicity parameter (e.g., assigning a different value to each OA  
256 component) will be a topic of future work.

257 The present work, thoroughly analyzes organic water uptake impacts over one  
258 simulated year (not just one month as done in Kakavas et al., 2022) and in quite a  
259 different geographical area (US here versus Europe in Kakavas et al., 2022). There are  
260 significant differences, but also similarities in the predicted changes and effects of SOA  
261 water. Both studies indicate that SOAW can contribute highly to the total PM<sub>1</sub> water  
262 and increase particulate nitrate concentrations especially in areas with high total nitrate  
263 concentrations. Pilinis et al. (1995) have argued that the single most important  
264 parameter in determining direct aerosol forcing is RH, and the most important process  
265 is the increase of the aerosol mass as a result of water uptake. They estimated that on  
266 average an increase of the RH from 40 to 80% for a global mean aerosol more than  
267 doubles the corresponding radiative forcing. As a result the inclusion of SOAW in  
268 future studies is highly recommended. ISORROPIA-lite provides a simple and  
269 computationally effective approach for the simulation of this SOAW.

270

271 **Code and Data Availability.** The model code and data used in this study are available  
272 from the authors upon request (spyros@chemeng.upatras.gr and  
273 athanasios.nenes@epfl.ch).

274

275 **Author Contributions.** SK incorporated ISORROPIA-lite in PMCAMx, carried out the  
276 simulations, analyzed the results and wrote the manuscript. SN and AN conceived and  
277 led the study and helped in the writing of the manuscript. All authors contributed to the  
278 reviewer responses and manuscript revisions.

279

280 **Competing Interests.** The authors declare no competing financial interest.

281

282 **Acknowledgements.** This work was supported by the project FORCeS funded from the  
283 European Union's Horizon 2020 research and innovation programme under grant  
284 agreement No 821205, and project PyroTRACH (ERC-2016-COG) funded from  
285 H2020-EU.1.1. - Excellent Science - European Research Council (ERC), project ID  
286 726165.

287

## 288 **References**

289 Baker, A., Kanakidou, M., Nenes, A., Myriokefalitakis, S., Croot, P.L., Duce, A. D.,  
290 Gao, Y., Guieu, C., Ito, A., Jickells, T. D., Mahowald, N. M., Middag, R.,  
291 Perron, M. M. G., Sarin, M. M., Shelley, R., and Turner, D. R.: Changing  
292 atmospheric acidity as a modulator of nutrient deposition and ocean  
293 biogeochemistry, *Sci. Adv.*, 7, doi: 10.1126/sciadv.abd8800, 2021.

294 Bian, Y. X., Zhao, C. S., Ma, N., Chen, J., and Xu, W. Y.: A study of aerosol liquid  
295 water content based on hygroscopicity measurements at high relative humidity  
296 in the North China Plain, *Atmos. Chem. Phys.*, 14, 6417–6426, 2014.

297 Bougiatioti, A., Nikolaou, P., Stavroulas, I., Kouvarakis, G., Weber, R., Nenes, A.,  
298 Kanakidou, M., and Mihalopoulos, N.: Particle water and pH in the eastern  
299 Mediterranean: source variability and implications for nutrient availability,  
300 *Atmos. Chem. Phys.*, 16, 4579–4591, 2016.

301 Carlton, A. G. and Turpin, B. J.: Particle partitioning potential of organic compounds  
302 is highest in the Eastern US and driven by anthropogenic water, *Atmos. Chem.*  
303 *Phys.*, 13, 10203–10214, 2013.

304 Chang, R. Y.-W., Slowik, J. G., Shantz, N. C., Vlasenko, A., Liggio, J., Sjostedt, S. J.,  
305 Leaitch, W. R., and Abbatt, J. P. D.: The hygroscopicity parameter ( $\kappa$ ) of  
306 ambient organic aerosol at a field site subject to biogenic and anthropogenic  
307 influences: relationship to degree of aerosol oxidation, *Atmos. Chem. Phys.*, 10,  
308 5047–5064, 2010.

309 Deetz, K., Vogel, H., Haslett, S., Knippertz, P., Coe, H., and Vogel, B.: Aerosol liquid  
310 water content in the moist southern West African monsoon layer and its  
311 radiative impact, *Atmos. Chem. Phys.*, 18, 14271–14295, 2018.

312 Donahue, N. M., Robinson, A. L., Stanier, C. O., and Pandis, S. N.: Coupled  
313 partitioning, dilution, and chemical aging of semivolatile organics, *Environ. Sci.*  
314 *Technol.*, 40, 2635–2643, 2006. *Environ: Comprehensive Air Quality Model*  
315 *with Extensions Version 4.40. Users Guide.* ENVIRON Int. Corp., Novato, CA,  
316 <http://www.camx.com>, 2006.

317 Fahey, K. and Pandis, S. N.: Optimizing model performance: variable size resolution  
318 in cloud chemistry modeling, *Atmos. Environ.*, 35, 4471–4478, 2001.

319 Fountoukis, C. and Nenes, A.: ISORROPIA II: a computationally efficient  
320 thermodynamic equilibrium model for  $K^+$ - $Ca^{2+}$ - $Mg^{2+}$ - $NH_4^+$ - $Na^+$ - $SO_4^{2-}$ - $NO_3^-$ -  
321  $Cl^-$ - $H_2O$  aerosols, *Atmos. Chem. Phys.*, 7, 4639–4659, 2007.

322 Fountoukis, C., Nenes, A., Sullivan, A., Weber, R., Van Reken, T., Fischer, M., Matías,  
323 E., Moya, M., Farmer, D., and Cohen, R. C.: Thermodynamic characterization  
324 of Mexico City aerosol during MILAGRO 2006, *Atmos. Chem. Phys.*, 9, 2141–  
325 2156, 2009.

326 Fountoukis, C., Megaritis, A. G., Skyllakou, K., Charalampidis, P. E.,  
327 Denier van der Gon, H. A. C., Crippa, M., Prévôt, A. S. H., Fachinger, F.,  
328 Wiedensohler, A., Pilinis, C., and Pandis, S. N.: Simulating the formation of  
329 carbonaceous aerosol in a European Megacity (Paris) during the MEGAPOLI  
330 summer and winter campaigns, *Atmos. Chem. Phys.*, 16, 3727–3741, 2016.

331 Freney, E. J., Sellegri, K., Canonaco, F., Colomb, A., Borbon, A., Michoud, V.,  
332 Doussin, J.-F., Crumeyrolle, S., Amarouche, N., Pichon, J.-M., Bourianne, T.,  
333 Gomes, L., Prevot, A. S. H., Beekmann, M., and Schwarzenböeck, A.:  
334 Characterizing the impact of urban emissions on regional aerosol particles:  
335 airborne measurements during the MEGAPOLI experiment, *Atmos. Chem.*  
336 *Phys.*, 14, 1397–1412, 2014.

337 Gopinath, A. K., Raj, S. S., Kommula, S. M., Jose, C., Panda, U., Bishambu, Y., Ojha,  
338 N., Ravikrishna, R., Liu, P., and Gunthe, S. S.: Complex interplay between  
339 organic and secondary inorganic aerosols with ambient relative humidity  
340 implicates the aerosol liquid water content over India during wintertime, *J. of*  
341 *Geophysical Research*, 127, e2021JD036430, 2022.

342 Gunthe, S. S., Liu, P., Panda, U., Raj, S. S., Sharma, A., Derbyshire, E., Reyes-Villegas  
343 E., Allan, J., Chen, Y., Wang, X., Song, S., Pöhlker, M. L., Shi, L., Wang, Y.,  
344 Kommula, S. M., Liu, T., Ravikrishna, R., McFiggans, G., Mickey, L. J.,  
345 Martin, S. T., Pöschl, U., Andreae, M. O., and Coe, H.: Enhanced aerosol  
346 particle growth sustained by high continental chlorine emission in India., *Nat.*  
347 *Geosci.*, 14, 77–84, 2021.

348 Guo, H., Xu, L., Bougiatioti, A., Cerully, K. M., Capps, S. L., Hite Jr., J. R., Carlton,  
349 A. G., Lee, S.-H., Bergin, M. H., Ng, N. L., Nenes, A., and Weber, R. J.: Fine-  
350 particle water and pH in the southeastern United States, *Atmos. Chem. Phys.*  
351 15, 5211–5228, 2015.

352 Guo, H., Liu, J., Froyd, K. D., Roberts, J. M., Veres, P. R., Hayes, P. L., Jimenez, J. L.,  
353 Nenes, A., and Weber, R. J.: Fine particle pH and gas–particle phase  
354 partitioning of inorganic species in Pasadena, California, during the 2010  
355 CalNex campaign, *Atmos. Chem. Phys.*, 17, 5703–5719, 2017.

356 Guo, H., Li, X., Li, W., Wu, J., Wang, S., and Wei, J.: Climatic modification effects on  
357 the association between PM<sub>1</sub> and lung cancer incidence in China, *BMC public*  
358 *health*, 21, 880, 2021.

359 Jathar, S.H., Mahmud, A., Barsanti, K.C., Asher, W. E.,  
360 Pankow, J. F., and Kleeman M. J.: Water uptake by organic aerosol and its  
361 influence on gas/particle partitioning of secondary organic aerosol in the United  
362 States, *Atmos. Environ.*, 129, 142–154, 2016.

362 Jin, X., Wang, Y., Li, Z., Zhang, F., Xu, W., Sun, Y., Fan, X., Chen, G., Wu, H., Ren,  
363 J., Wang, Q., and Cribb, M.: Significant contribution of organics to aerosol  
364 liquid water content in winter in Beijing, China, *Atmos. Chem. Phys.*, 20, 901–  
365 914, 2020.

366 Kakavas, S., Pandis, S. N., and Nenes, A.: ISORROPIA-lite: A comprehensive  
367 atmospheric aerosol thermodynamics module for Earth System Models, *Tellus*  
368 *B*, 74, 1–23, 2022.

369 Karamchandani, P., Vijayaraghavan, K., and Yarwood, G.: Sub-grid scale plume  
370 modeling, *Atmosphere*, 2, 389–406, 2011.

371 Karydis, V. A., Tsimpidi, A. P., Fountoukis, C., Nenes, A., Zavala, M., Lei, W., Molina,  
372 L. T., and Pandis, S. N.: Simulating the fine and coarse inorganic particulate  
373 matter concentrations in a polluted megacity, *Atmos. Environ.*, 44, 608–620,  
374 2010.

375 Kodros, J. K., Papanastasiou, D. K., Paglione, M., Masiol, M., Squizzato, S., Florou,  
376 K., Skyllakou, K., Kaltsonoudis, C., Nenes, A., and Pandis, S. N.: Rapid dark  
377 aging of biomass burning as an overlooked source of oxidized organic aerosol.,  
378 *Proc. Natl. Acad. Sci. U.S.A.*, 117, 33028–33033, 2020.

379 Koehler, K. A., Kreidenweis, S. M., DeMott, P. J., Petters, M. D., Prenni, A. J., and  
380 Carrico, C. M.: Hygroscopicity and cloud droplet activation of mineral dust  
381 aerosol, *Geoph. Res. Lett.*, 36, (8), 2009.

382 Koo, B., Pandis, S. N., and Ansari, A.: Integrated approaches to modeling the organic  
383 and inorganic atmospheric aerosol components, *Atmos. Environ.*, 37, 4757-  
384 4768, 2003.

385 Kostenidou, E., Pathak, R. K., and Pandis, S. N.: An algorithm for the calculation of  
386 secondary organic aerosol density combining AMS and SMPS data, *Aerosol  
387 Sci. Technol.*, 41, 1002–1010, 2007.

388 Kuang, Y., Zhao, C. S., Zhao, G., Tao, J. C., Xu, W., Ma, N., and Bian, Y. X.: A novel  
389 method for calculating ambient aerosol liquid water content based on  
390 measurements of a humidified nephelometer system, *Atmospheric  
391 Measurement Techniques*, 11, 2967–2982, 2018.

392 Kuang, Y., Xu, W., Tao, J., Ma, N., Zhao, C., and Shao, M.: A review on laboratory  
393 studies and field measurements of atmospheric organic aerosol hygroscopicity  
394 and its parameterization based on oxidation levels, *Current Pollution Reports*,  
395 10.1007/s40726-020-00164-2, 2020. Li, X., Song, S., Zhou, W., Hao, J.,  
396 Worsnop, D. R., and Jiang, J.: Interactions between aerosol organic components  
397 and liquid water content during haze episodes in Beijing, *Atmos. Chem. Phys.*,  
398 19, 12163–12174, 2019.

399 Li, J., Zhang, H., Ying, Q., Wu, Z., Zhang, Y., Wang, X., Li, X., Sun, Y., Hu, M.,  
400 Zhang, Y., and Hu, J.: Impacts of water partitioning and polarity of organic  
401 compounds on secondary organic aerosol over eastern China, *Atmos. Chem.  
402 Phys.*, 20, 7291–7306, 2020.

403 Liao, H. and Seinfeld, J. H.: Global impacts of gas-phase chemistry aerosol interactions  
404 on direct radiative forcing by anthropogenic aerosols and ozone, *J. Geophys.*  
405 *Res.*, 110, D18208, 2005.

406 Metzger, S., Mihalopoulos, N., and Lelieveld, J.: Importance of mineral cations and  
407 organics in gas-aerosol partitioning of reactive nitrogen compounds: case study  
408 based on MINOS results., *Atmos. Chem. Phys.*, 6, 2549–2567, 2006.

409 Murphy, B. N. and Pandis, S. N.: Exploring summertime organic aerosol formation in  
410 the Eastern United States using a regional-scale budget approach and ambient  
411 measurements, *J. Geophys. Res.*, 115, D24216, 2010.

412 Nenes, A., Pandis, S. N., Weber, R. J., and Russell, A.: Aerosol pH and liquid water  
413 content determine when particulate matter is sensitive to ammonia and nitrate  
414 availability, *Atmos. Chem. Phys.*, 20, 3249–3258, 2020.

415 Nenes, A., Pandis, S. N., Kanakidou, M., Russell, A. G., Song, S., Vasilakos, P., and  
416 Weber, R. J.: Aerosol acidity and liquid water content regulate the dry  
417 deposition of inorganic reactive nitrogen, *Atmos. Chem. Phys.*, 21, 6023–6033,  
418 2021. Nguyen, T. K. V., Zhang, Q., Jimenez, J. L., Pike, M., and Carlton, A. G.:  
419 Liquid water: ubiquitous contributor to aerosol mass. *Environ. Sci. Tech. Let.*,  
420 3, 257–263, 2016.

421 Pandis, S. N. and Seinfeld, J. H.: Sensitivity analysis of a chemical mechanism for  
422 aqueous-phase atmospheric chemistry, *J. Geophys. Res.*, 94, 1105–1126, 1989.

423 Pandis, S. N., Wexler, A. S., and Seinfeld, J. H.: Secondary organic aerosol formation  
424 and transport – II. Predicting the ambient secondary organic aerosol size  
425 distribution, *Atmos. Environ.*, 27, 2403–2416, 1993.

426 Petters, M. D., Prenni, A. J., Kreidenweis, S. M., DeMott, P. J., Matsunaga, A., Lim,  
427 Y. B., and Ziemann, P. J.: Chemical aging and the hydrophobic-to-hydrophilic  
428 conversion of carbonaceous aerosol, *Geophys. Res. Lett.*, 33, L24806, 2006.

429 Petters, M. D. and Kreidenweis, S. M.: A single parameter representation of  
430 hygroscopic growth and cloud condensation nucleus activity, *Atmos. Chem.*  
431 *Phys.*, 7, 1961–1971, 2007.

432 Pilinis, C., Pandis, S. N., and Seinfeld, J. H.: Sensitivity of direct climate forcing by  
433 atmospheric aerosols to aerosol size and composition, *Journal of Geophysical*  
434 *Research*, 100, 18739, 1995.

435 Pye, H. O. T., Nenes, A., Alexander, B., Ault, A. P., Barth, M. C., Clegg, S. L., Collett  
436 Jr, J. L., Fahey, K. M., Hennigan, C. J., Herrmann, H., Kanakidou, M., Kelly, J.

437 T., Ku, I.-T., McNeill, V. F., Riemer, N., Schaefer, T., Shi, G., Tilgner, A.,  
438 Walker, J. T., Wang, T., Weber, R., Xing, J., Zaveri, R. A., and Zuend, A.: The  
439 acidity of atmospheric particles and clouds, *Atmos. Chem. Phys.*, 20, 4809–  
440 4888, 2020.

441 Seinfeld, J. H. and Pandis, S. N.: *Atmospheric chemistry and physics: From air*  
442 *pollution to climate change*, Wiley: New York, 2006.

443 Skyllakou, K., Murphy, B. N., Megaritis, A. G., Fountoukis, C., and Pandis, S. N.:  
444 Contributions of local and regional sources to fine PM in the megacity of Paris,  
445 *Atmos. Chem. Phys.*, 14, 2343–2352, 2014.

446 Skyllakou, K., Rivera, P. G., Dinkelacker, B., Karnezi, E., Kioutsioukis, I., Hernandez,  
447 C., Adams, P. J., and Pandis, S. N.: Changes in PM<sub>2.5</sub> concentrations and their  
448 sources in the US from 1990 to 2010, *Atmos. Chem. Phys.*, 21, 17115–17132,  
449 2021.

450 Song, S., Gao, M., Xu, W., Shao, J., Shi, G., Wang, S., Wang, Y., Sun, Y., and McElroy,  
451 M. B.: Fine-particle pH for Beijing winter haze as inferred from different  
452 thermodynamic equilibrium models, *Atmos. Chem. Phys.*, 18, 7423–7438,  
453 2018.

454 Strader, R., Gurciullo, C., Pandis, S. N., Kumar, N., and Lurmann, F. W.: Development  
455 of gas-phase chemistry, secondary organic aerosol, and aqueous-phase  
456 chemistry modules for PM modeling, Final report for CRC Project A21-1  
457 prepared for the Coordinating Research Council, Atlanta, GA by Sonoma  
458 Technology, Inc., Petaluma, CA, 1998.

459 Sun, X., Ivey, C. E., Baker, K. R., Nenes, A., Lareau, N. P., and Holmes, H. A.:  
460 Confronting Uncertainties of Simulated Air Pollution Concentrations during  
461 Persistent Cold Air Pool Events in the Salt Lake Valley, Utah., *Environ. Sci.*  
462 *Technol.*, 55, 15072–15081, 2021.

463 Tsimpidi, A. P., Karydis, V. A., Zavala, M., Lei, W., Molina, L., Ulbrich, I. M.,  
464 Jimenez, J. L., and Pandis, S. N.: Evaluation of the volatility basis-set approach  
465 for the simulation of organic aerosol formation in the Mexico City metropolitan  
466 area, *Atmos. Chem. Phys.*, 10, 525–546, 2010.

467 Turpin, B. J. and Lim, H. J.: Species Contributions to PM<sub>2.5</sub> Mass Concentrations:  
468 Revisiting Common Assumptions for Estimating Organic Mass, *Aerosol Sci.*  
469 *Technol.*, 35, (1), 602–610, 2001.

470 Wu, Z., Wang, Y., Tan, T., Zhu, Y., Li, M., Shang, D., Wang, H., Lu, K., Guo, S., Zeng,  
471 L., and Zhang, Y.: Aerosol liquid water driven by anthropogenic inorganic salts:  
472 Implying its key role in haze formation over the North China Plain, *Environ.*  
473 *Science & Technology Letters*, 10.1021/acs.estlett.8b00021, 2018.

474 Xing, J., Pleim, J., Mathur, R., Pouliot, G., Hogrefe, C., Gan, C.-M., and Wei, C.:  
475 Historical gaseous and primary aerosol emissions in the United States from  
476 1990 to 2010, *Atmos. Chem. Phys.*, 13, 7531–7549, 2013.

477 Yarwood, G., Rao, S., Yocke, M., and Whitten, G. Z.: Updates to the Carbon Bond  
478 Chemical Mechanism: CB05, Research Triangle Park, [https://camx-  
479 wp.azurewebsites.net/Files/CB05\\_Final\\_Report\\_120805.pdf](https://camx-wp.azurewebsites.net/Files/CB05_Final_Report_120805.pdf), 2005.

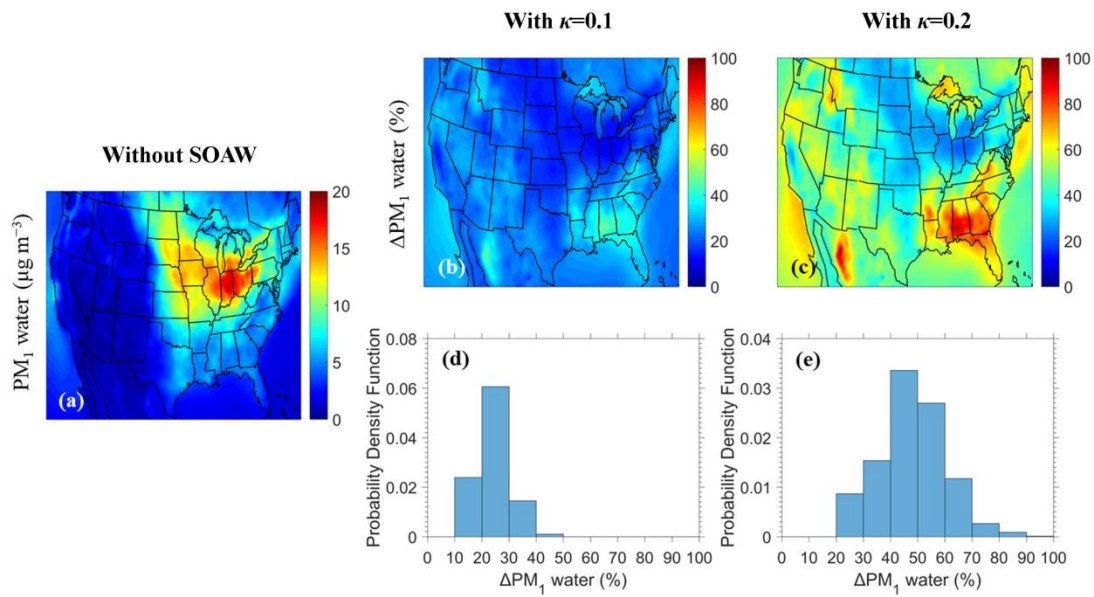
480 Zakoura, M. and Pandis, S. N.: Improving fine aerosol nitrate predictions using a  
481 Plume-in-Grid modeling approach, *Atmos. Environ.*, 215, 116887, 2019.

482 Zhang, Q. J., Beekmann, M., Drewnick, F., Freutel, F., Schneider, J., Crippa, M.,  
483 Prevot, A. S. H., Baltensperger, U., Poulain, L., Wiedensohler, A., Sciare, J.,  
484 Gros, V., Borbon, A., Colomb, A., Michoud, V., Doussin, J.-F., Denier van der  
485 Gon, H. A. C., Haeffelin, M., Dupont, J.-C., Siour, G., Petetin, H., Bessagnet,  
486 B., Pandis, S. N., Hodzic, A., Sanchez, O., Honoré, C., and Perrussel, O.:  
487 Formation of organic aerosol in the Paris region during the MEGAPOLI  
488 summer campaign: evaluation of the volatility basis-set approach within the  
489 CHIMERE model, *Atmos. Chem. Phys.*, 13, 5767–5790, 2013.

490  
491  
492  
493  
494  
495  
496  
497  
498  
499  
500  
501  
502  
503  
504  
505



507



508

509

510 **Figure 1.** Maps of: (a) annual average PM<sub>1</sub> water ground-level concentrations  
511 neglecting SOAW, (b) annual average fractional increase of PM<sub>1</sub> water when SOAW  
512 is present in the simulations with  $\kappa=0.1$  and, (c) with  $\kappa=0.2$  during 2010. The probability  
513 density as a function of fractional increase in the annual PM<sub>1</sub> water concentrations due  
514 to SOAW when: (d)  $\kappa=0.1$  and (e)  $\kappa=0.2$  is shown.

515

516

517

518

519

520

521

522

523

524

525

526

527

528

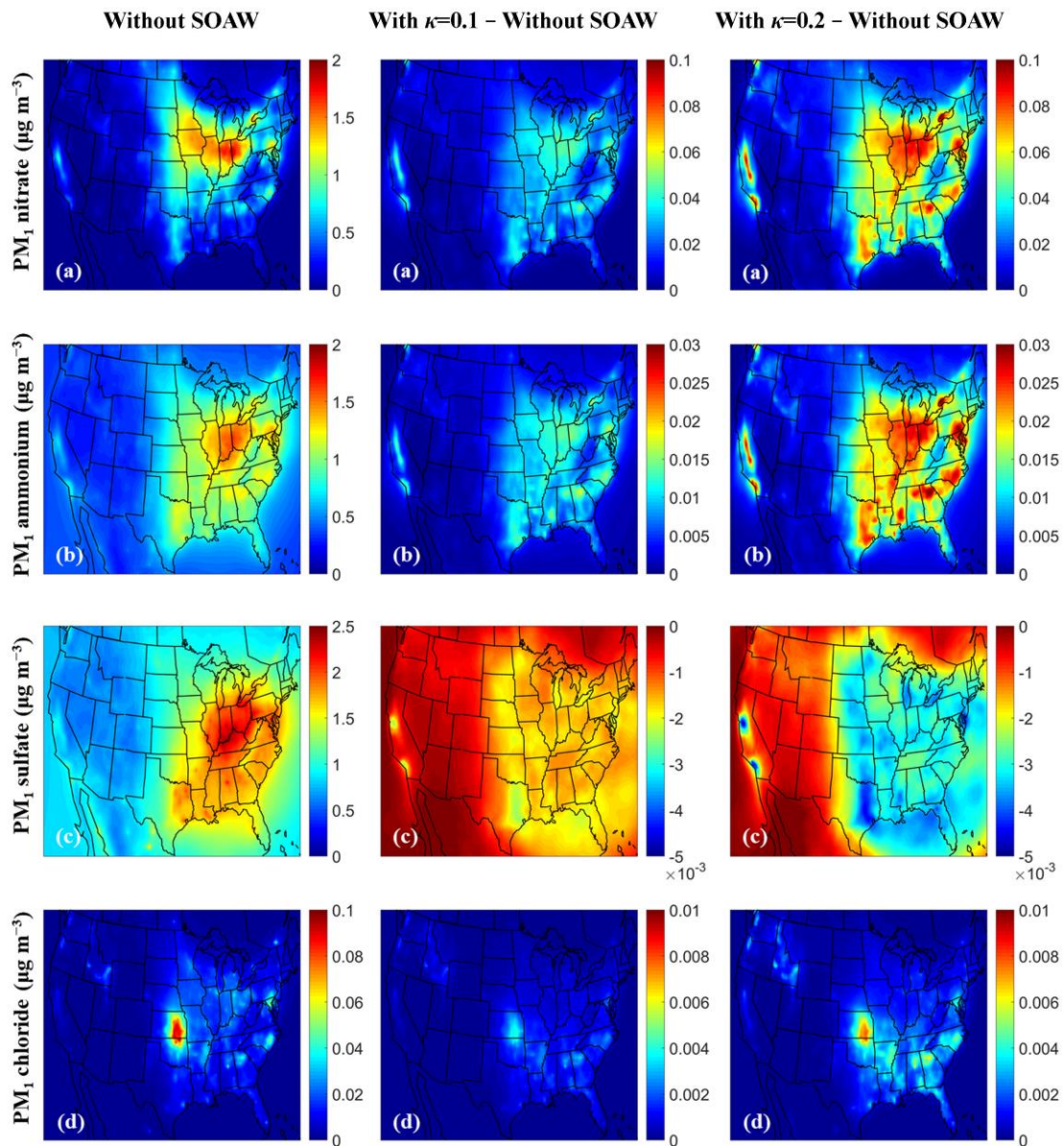
529

530

531

532

533



534

535

536 **Figure 2.** Annual average ground-level concentrations (in  $\mu\text{g m}^{-3}$ ) of PM<sub>1</sub>: (a) nitrate,  
 537 (b) ammonium, (c) sulfate, and (d) chloride neglecting SOAW and the annual  
 538 concentration changes when SOAW is present in the simulations with  $\kappa=0.1$  and  $\kappa=0.2$ .  
 539 A positive change corresponds to an increase. A negative change corresponds to a  
 540 decrease.

541

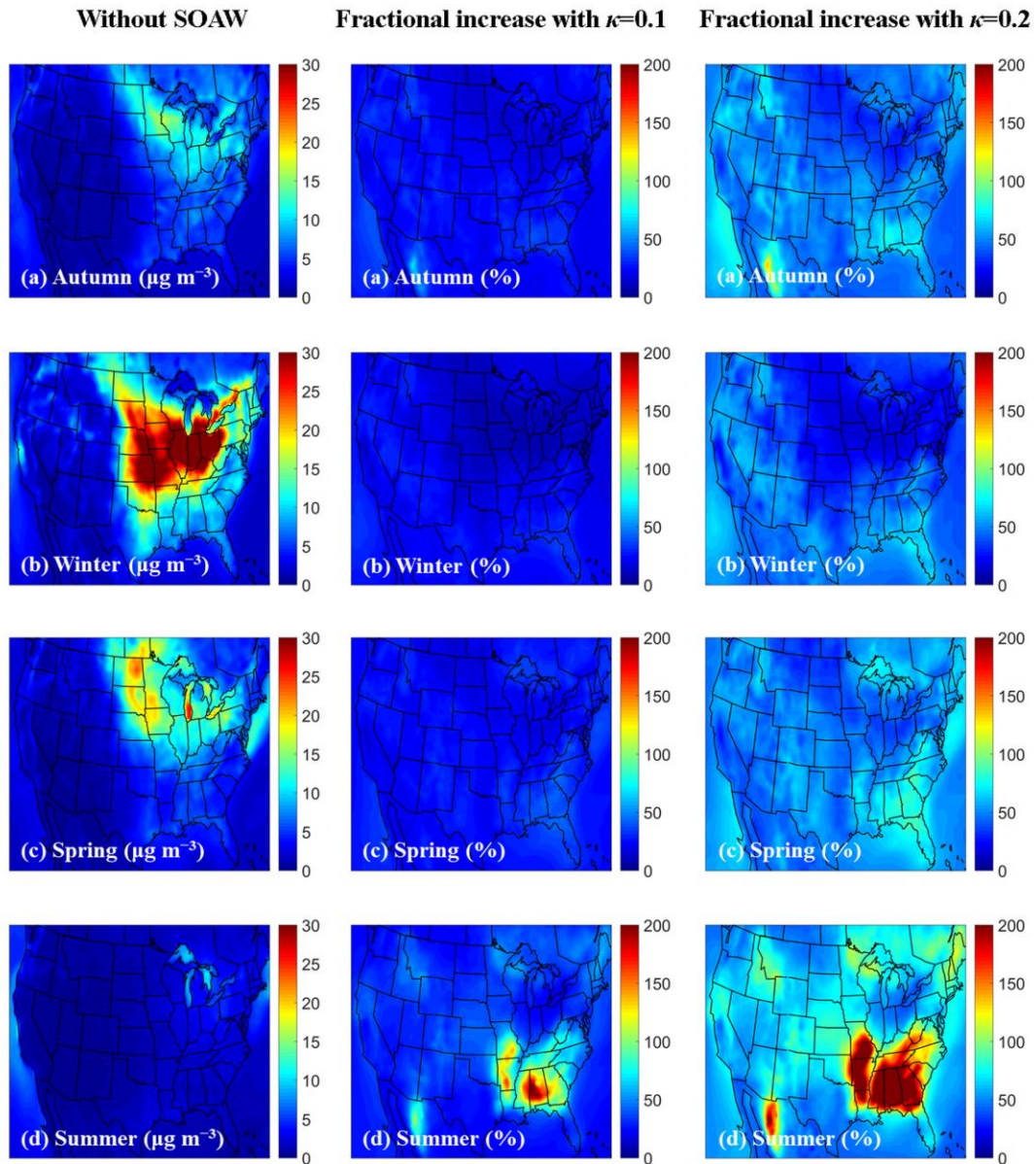
542

543

544

545

546



547

548

549 **Figure 3.** Average ground-level concentrations of  $\text{PM}_{10}$  water neglecting SOAW (in  $\mu\text{g}$   
 550  $\text{m}^{-3}$ ) and the fractional increase when SOAW is present in the simulations with  $\kappa=0.1$   
 551 and  $\kappa=0.2$  during: (a) autumn (SON), (b) winter (DJF), (c) spring (MAM), and (d)  
 552 summer (JJA) of 2010.

553

554

555

556

557

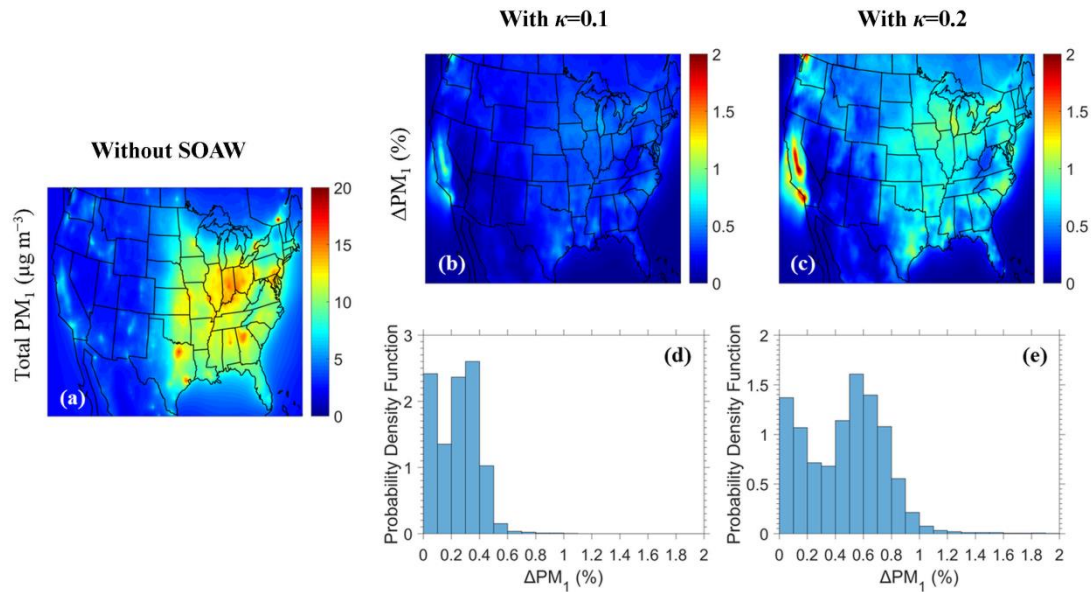
558

559

560

561

562



563

564

565 **Figure 4.** Maps of: (a) annual average total dry PM<sub>1</sub> ground-level concentrations  
566 neglecting SOAW, (b) annual average fractional increase of total dry PM<sub>1</sub> when SOAW  
567 is present in the simulations with  $\kappa=0.1$  and, (c) with  $\kappa=0.2$  during 2010. The probability  
568 density as a function of fractional increase in the annual total dry PM<sub>1</sub> concentrations  
569 due to SOAW when: (d)  $\kappa=0.1$  and (e)  $\kappa=0.2$  is shown.

570

571

572

573

574

575

576

577

578

579

580

581

582

583

584

585

586

587

588

589

590

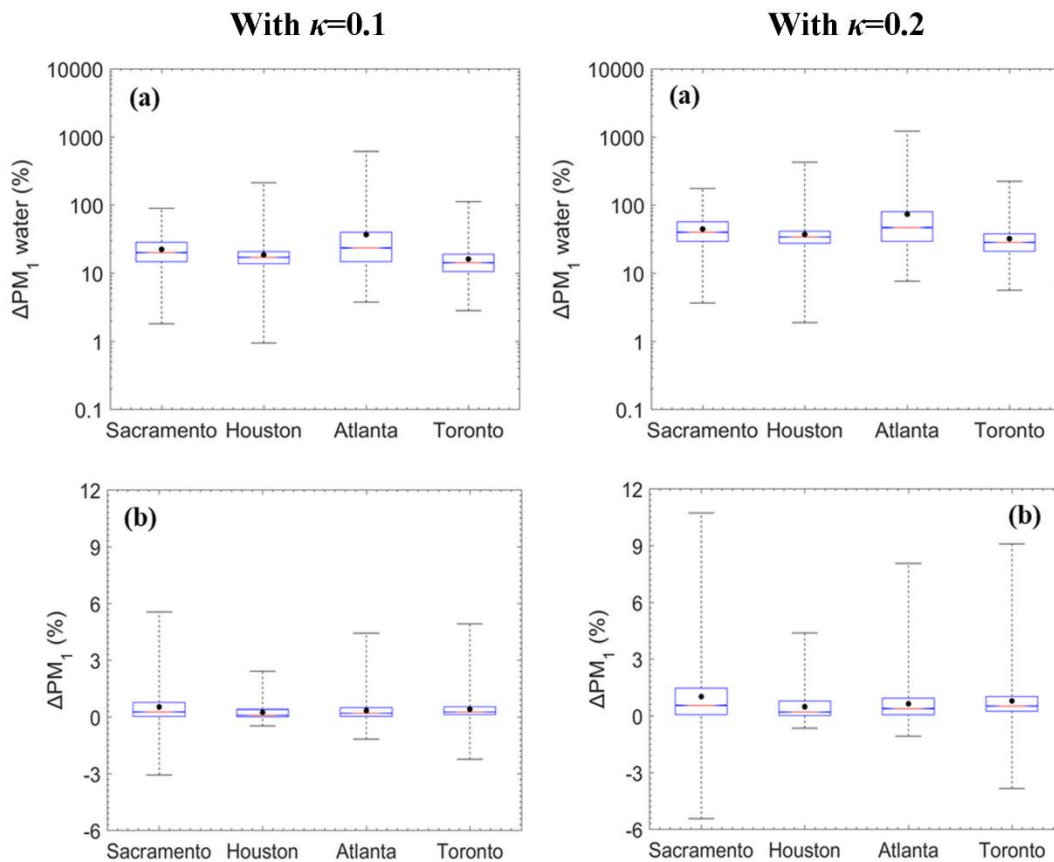
591

592

593

594

595



596

597

598 **Figure 5.** Box plots for fractional change in the hourly: (a) PM<sub>1</sub> water and (b) total dry  
599 PM<sub>1</sub> due to SOAW when  $\kappa=0.1$  and  $\kappa=0.2$  for Sacramento, California; Houston, Texas;  
600 Atlanta, Georgia; and Toronto, Canada during 2010. The red line represents the median,  
601 the black dot is the mean value, the upper box line is the upper quartile (75%) and the  
602 lower box line is the lower quartile (25%) of the distribution. A negative change  
603 corresponds to a decrease.

604

605

606

607

608

609

610

611

612

613

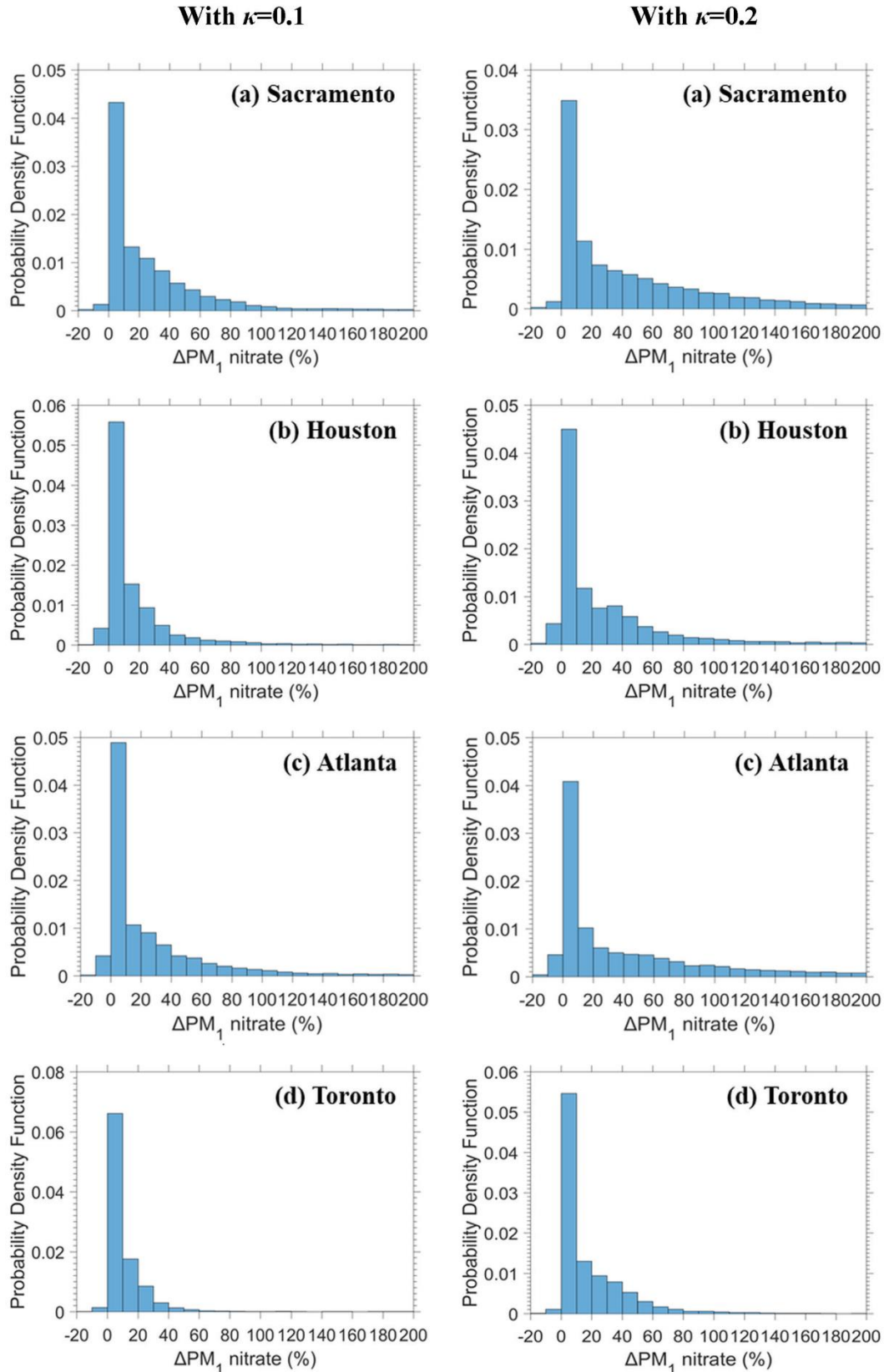
614

615

616

617

618



619  
620

621 **Figure 6.** The probability density as a function of fractional increase in the hourly  $PM_1$   
622 nitrate due to SOAW when  $\kappa=0.1$  and  $\kappa=0.2$  for: (a) Sacramento, California; (b)  
623 Houston, Texas; (c) Atlanta, Georgia; and (d) Toronto, Canada during 2010.